Zhang, P.; Behl, M.; Peng, X.; Razzaq, M.; Lendlein, A.:
Ultrasonic Cavitation Induced Shape-Memory Effect in Porous Polymer Networks.
In: Macromolecular Rapid Communications. Vol. 37 (2016) 23, 1897 - 1903.

First published online by Wiley: 26.09.2016

https://dx.doi.org/10.1002/marc.201600439

Ultrasonic Cavitation Induced Shape-memory Effect in Porous Polymer Networks

Pengfei Zhang, Marc Behl, Xingzhou Peng, Muhammad Yasar Razzaq, and Andreas Lendlein*

———

P. Zhang, Dr. M. Behl, X. Peng, Dr. M. Razzaq, Prof. A. Lendlein
Institute of Biomaterial Science, Helmholtz-Zentrum Geesthacht, Kantstr. 55, 14513, Teltow, Germany
P. Zhang, X. Peng, Prof. A. Lendlein
Institute of Chemistry, University of Potsdam, Karl-Liebknecht-Str. 24-25, 14469 Potsdam, Germany
P. Zhang, Dr. M. Behl, X. Peng, Prof. A. Lendlein
Tianjin University-HZG Research Center Joint Laboratory for Biomaterials and Regenerative Medicine, Weijin Road 92, 300072 Tianjin (China) and Kantstr. 55, 14513 Teltow, Germany E-mail: andreas.lendlein@hzg.de

———

Abstract: Inspired by the application of ultrasonic cavitation based mechanical force (CMF) to open small channels in natural soft materials (skin or tissue), we explored whether an artificial polymer network can be created, which shape-changes can be induced by CMF. Our concept comprises an interconnected macro-porous rhodium-phosphine (Rh-P) coordination polymer network, in which a CMF can reversibly dissociate the Rh-P micro-phases. In this way, the ligand exchange of Rh-P coordination bonds in polymer network is accelerated, resulting in a topological rearrangement of molecular switches. This rearrangement of molecular switches enables the polymer network to release internal tension under ultrasound exposure, resulting in a CMF-induced shape-memory capability. The interconnected macro-porous structure with thin pore walls is essential for allowing the CMF to effectively permeate throughout the polymer network. Potential applications of this CMF-induced shape-memory polymer could be mechano-sensors or ultrasound controlled switches.

1. Introduction

Ultrasound is an efficient tool to generate local mechanical force in liquid media by cavitation.[1-3] The process of cavitation involves the formation of a gas bubble in the liquid, increase of the bubble size as the ultrasound wave passes through the media, and finally collapse of the bubble when the bubble exceeds a critical size.[2] This collapse of bubbles can result in shock waves with a velocity around 1000 $m \cdot s^{-1}$ in liquid media or generate micro-jets (velocity: several 100 $m \cdot s^{-1}$) directed towards the solid surface.[4-5] When the collapse occurs near solid-liquid boundary, a strong mechanical force can be generated. Owing to the fascinating advantages such as ease of fabrication, and eco-friendliness, the cavitation based mechanical force (CMF) has been extensively utilized for medical applications in natural soft materials (skin or brain). The shock waves or micro-jets are capable to disorder the lipid-bilayer in skin, which causes an increase of the skin permeability and thus enhances the transdermal transport of drug or protein across the skin.[6-7] This cavitation effect was also utilized to reversibly disrupt the blood-brain barrier by cleavage of tight junctions present between the capillary endothelial cells to enhance the efficiency of drug delivery to brain.[8] Furthermore, CMF is also attractive in chemistry to accelerate the exchange rate of supramolecular interactions or site-specific cleavage of weak dynamic covalent bonds.[3, 9-12] Cleavage or exchange reactions usually requiring high temperature can be achieved near ambient or even at lower temperatures under application of CMF.[2-3]

Inspired by the above-mentioned backgrounds and the demand for ultrasound-sensitive shape-shifting polymers,[13-16] we explored whether a CMF-induced shape-memory effect (SME) can be created in artificial polymers. Considering the characteristics of CMF, these CMF-triggered shape-memory polymers (SMP) could be interesting candidates as mechano-sensors or ultrasound controlled switches, which apply in specific environments (e.g. constant ambient or lower

temperature, light avoiding). As ultrasonic cavitation occurs dominantly at the surface of solid polymers,[2, 5] a key challenge was the design of an appropriate material structure, which enables the CMF to effectively permeate throughout the bulk polymer sample. In addition, the selection of suitable molecular switches (temporary crosslinks) is critical as well.[14, 17-19] The temporary crosslinks must exhibit mechano-responsivity during sonication (to enable the shape recovery) and need to provide a temporary stability (to enable fixation of the temporary shape).

We address these challenges by the design of an interconnected macro-porous polymer network that contained rhodium(I)-phosphine coordination bonds (Rh-PCBs) as well as covalent netpoints (chemical structure shown in Scheme 1a). The interconnected macro-porous structure with thin porous walls provides a large specific surface area. Moreover, the interconnected structure allows the penetration of ultrasound waves through the interconnected pores, which can induce the collapse of cavitation bubbles inside the macro-pores and hence improve the efficiency of energy input from ultrasound to the polymer. To ensure the collapse of cavitation bubbles inside of the macro-pores the size of macro-pores in polymer network must be larger than the critical collapse size of cavitation bubbles. In addition, low frequency ultrasound (LU, frequency = 20 kHz) was selected because the cavitation bubbles are the most prone to be generated or to grow at a frequency of 20 kHz,[2] enabling the highest cavitation intensity. Rh-PCBs were employed as mechanically sensitive molecular switches, because of the ligand-exchange kinetics (Scheme 1b) and the high coordination stoichiometry (each rhodium ion is able to coordinate up to three or four phosphine ligands, resulting in a relatively high stability).[12, 20] We expected that the Rh-PCBs are capable to fix the temporary shape and control the shape recovery upon LU treatment. Poly(*n*-butyl acrylate) (P*n*-BA) was employed as the compound for the elastic polymer backbone and poly(propylene glycol) dimethacrylate (PPGDMA, M_n = 560 g·mol^{-1}) provided the covalent netpoints (hard

domains). Water fixed near ambient temperature (18 ± 1 °C) was employed as ultrasonic medium to prevent heating of the polymer during LU treatment (Figure S1).

We hypothesized that such a material would provide a morphology, in which the rhodium-phosphine complexes micro-phase separate from the phase provided by the polymer backbone, so that both the Rh-PCBs and their aggregates of micro-phase act as molecular switches. In such a setting the CMF could dissociate the aggregates of the micro-phase separated morphology of rhodium-phosphine complexes and accelerate the ligand exchange rate of Rh-PCBs. Considering the cavitation induced strong violent micro-jets and the large specific surface area as well as thin porous walls of interconnected macro-porous polymer network, the CMF could impact/deform the thin porous wall during sonication and thus result in the dissociation of the aggregates of the micro-phase separated morphology or would accelerate the ligand exchange rate of Rh-PCBs in the inside of porous wall. In this way, as illustrated in Scheme 1c, when a deformed macro-porous polymer network under application of an external force is treated by LU, the accelerated ligand exchange enables the topology of molecular switches in the polymer network to undergo a rapid rearrangement, which induces the deformed polymer backbones to reach their favored entropic state (stress relaxation). Upon removal of LU, the ligand exchange rate decrease again while at the same time the rhodium-phosphine micro-phase separated morphology re-aggregates, enabling fixation of the temporary shape. Further exposure to LU results in the re-dissociation of micro-phase separated morphology and increase of ligand exchange rate of Rh-PCBs, and enable the polymer network to return its permanent shape set by the covalent netpoints due to the entropy elasticity.

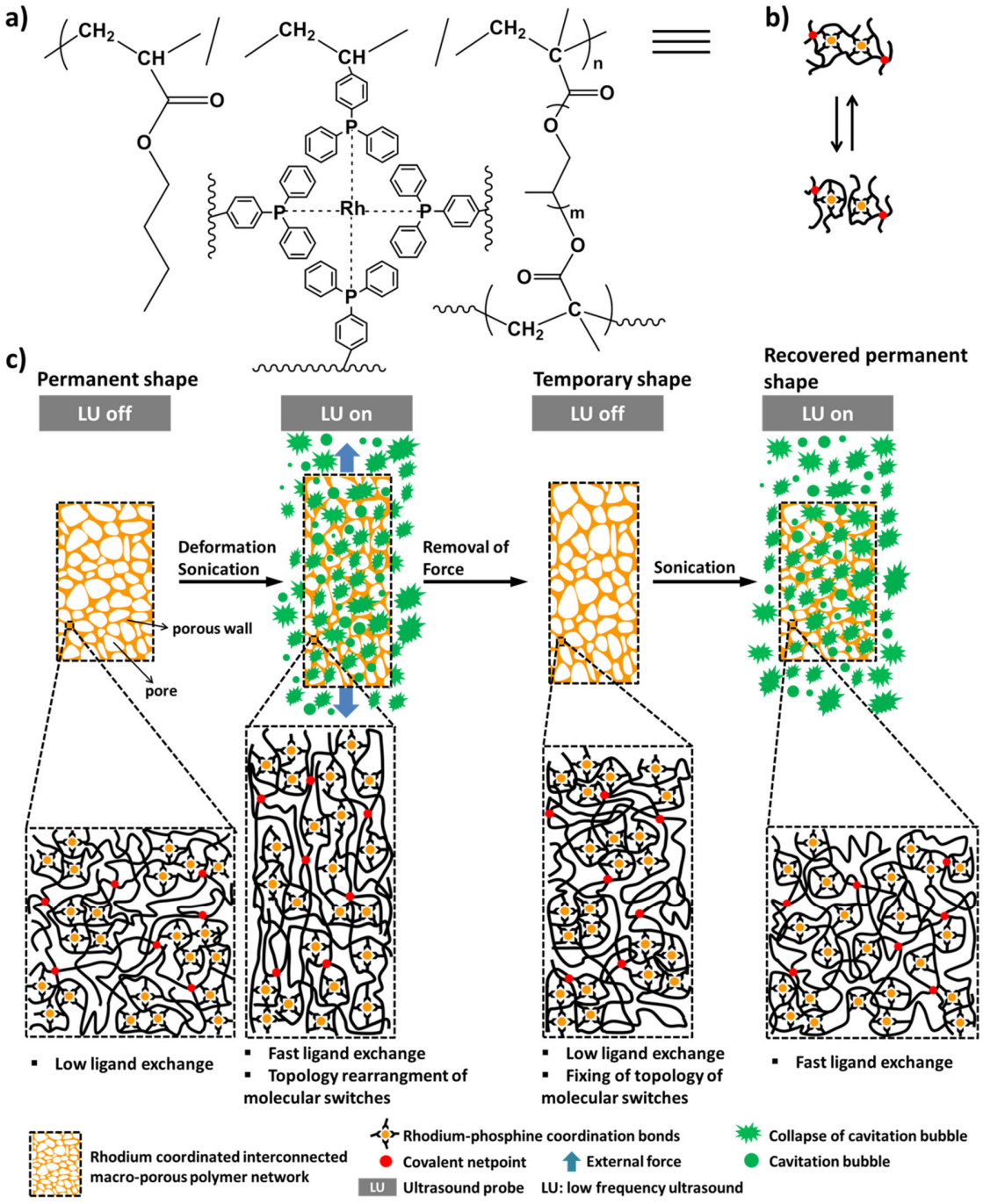

Scheme 1. a) Chemical structure of rhodium coordinated interconnected macro-porous polymer network. b) Schematic illustration of the ligand-exchange of rhodium-phosphine coordination bonds. c) Schematic illustration of proposed shape-memory mechanism of the rhodium coordinated interconnected macro-porous polymer network.

2. Results and Discussion

To fulfill the requirements listed above, an interconnected macro-porous poly[(*n*-BA)-*co*-DPPST-*co*-PPGDMA] network (named as: IMP-D(*x*), *x* indicates the molar concentration of DPPST (diphenylphosphinostyrene) feed, which was varied between 5 mol% and 13 mol%, the PPGDMA feed is constant 0.0625 mol%) was prepared (Figure S2, and Table S1, S2). Afterwards, the IMP-D(*x*) was coordinated with $[RhCl(COD)]_2$, from which the bulk, targeted rhodium coordinated interconnected macro-porous polymer network was obtained (named as: Rh-IMP-D(*x*)). The interconnected macro-porous structure was confirmed by scanning electron microscope (SEM, Figure S3). In the synthesized Rh-IMP-D(*x*), the pore size ranged between 200 and 400 μm (larger than the critical collapse size of cavitation bubbles in water (170 μm)), and the wall thickness ranged between 5 and 25 μm. The absorbance at 410 nm in UV-VIS spectra of Rh-IMP-D(*7*) verified the existence of Rh-PCBs in Rh-IMP-D(*x*) (Figure S4). The appearance of diffraction peak ($s = 0.043\ nm^{-1}$) of Rh-IMP-D(*11*) in small angle X-ray scattering (SAXS, Figure S5) and $2\theta = 6.9°$ in wide angle X-ray scattering (WAXS, Figure S6) confirmed the micro-phase separated morphology in Rh-IMP-D(*x*). Additionally, the IMP-D(*x*) and the Rh-IMP-D(*x*) displayed a glass transition temperature (T_g) around -45 °C (Figure S7, Table S3). Furthermore, the values of Young's modulus (*E*) of Rh-IMP-D(*x*) (*E*: ranged between 1.0 and 8.5 MPa) were one order of magnitude higher than those of the IMP-D(*x*) (*E*: ranged between 0.2 and 0.5 MPa) (Table S3), suggesting that the formation of Rh-PCBs caused an increasing of crosslink density. Moreover, water-uptake experiments confirmed the hydrophobicity of Rh-IMP-D(*x*) (Figure S8).

In Rh-IMP-D(*x*), the Rh-PCBs and their separated micro-phases were designed as mechanically sensitive molecular switches (temporary crosslinks). We assumed that upon LU treatment, the

CMF would dissociate the aggregates of the micro-phase separated morphology, which can result in a decrease of crosslink density in Rh-IMP-D(*x*) and thus decrease in mechanical strength. Upon removal of LU, the dissociated micro-phase separated morphology can re-aggregate in Rh-IMP-D(*x*), resulting in a reversible increase of the mechanical strength of Rh-IMP-D(*x*). To prove this assumption, the storage moduli (*G'*) of Rh-IMP-D(*x*) before LU and after LU treatment were examined by a rheometer. Because of the porous structure of as well as the hydrophobicity (non-swelling in water) of the Rh-IMP-D(*x*), LU treatment will induce the residual water in pores. To ensure that the change in mechanical strength is directly caused by the dissociation of micro-phase aggregates by CMF, the residual water in pores of Rh-IMP-D(*x*) should be removed before mechanical testing. Owing to the hydrophobicity of Rh-IMP-D(*x*), the residual water can be completely removed by a filter paper and applying vacuum (around 200 mbar, 4 min) treatment, and the successful removal of water was proved by determining of weight and by attenuated total reflectance-fourier transform infrared spectroscopy (ATR-FTIR, Figure S9), to determine the bands attributed to water). The frequency-dependent storage moduli (*G'*) of Rh-IMP-D(*9*) are shown in Figure 1a. In the frequency ranging of 1-10 Hz, the *G'* values of Rh-IMP-D(*9*) after LU treatment (ranging between 30 kPa and 58 kPa) showed a significant decrease compared to those before LU treatment (ranging between 62 kPa and 100 kPa). After removal of LU, the *G'* values displayed a reversible increase and reached equilibrium after 6 h. The same tendency of reversible increase of *G'* values can be also observed in Rh-IMP-D(*11*) and Rh-IMP-D(*7*) (Figure S10). These results implied the reversible dissociation of micro-phase aggregates. In addition, it is essential to clarify whether the mechanical force generated from the rheometer can induce the dissociation of micro-phase aggregates in Rh-IMP-D(x). Therefore, the *G'* values of Rh-IMP-D(x) before LU treatment were measured for two times. The *G'* values from the second measurement

did almost not change compared to those from the first measurement, confirming that the dissociation of micro-phase aggregates in Rh-IMP-D(x) is caused by CMF. Moreover, the morphology of Rh-IMP-D(*7*) after LU treatment were investigated by SAXS (Figure S11) and WAXS (Figure S12). Almost no shift of diffraction peak can be observed in both SAXS pattern and WAXS pattern of the Rh-IMP-D(*7*) after LU treatment compared to the Rh-IMP-D(*7*) before LU treatment, suggesting the reversible aggregation of micro-phase separated morphology.

We also hypothesized that the cavitation can accelerate the ligand exchange rate of Rh-PCBs. To verify this concept, we designed a "rhodium ion diffusion" experiment (Figure 1b). We prepared a poly[(*n*-BA)-*co*-DPPST-*co*-PPGDMA] film (DPPST composition: 7 mol%, film thickness: 0.3 mm, named as: PF) and a rhodium coordinated poly[(*n*-BA)-*co*-DPPST-*co*-PPGDMA] film (named as: Rh-PF). In this experiment, the surface of Rh-PF was treated by LU (amplitude: 80%, 3 min, in water at constant 18 ± 1 °C). Afterwards, the PF was superimposed on the LU treated surface of Rh-PF by a compression of 15%. This bilayer material was kept at 18 °C for 6 h. Finally, the treated-PF(a) was obtained. As a control, Rh-PF (without any treatment) and PF were superimposed by a compression of 15% at 18 °C for 6 h, from which the treated-PF(b) was obtained. The "rhodium ion diffusion" experiment is based on the assumption that the ligand exchange kinetics could induce the diffusion of rhodium ions from Rh-PF to PF through the interface and thus formation of Rh-PCBs in treated-PF. UV-VIS spectra were used to confirm the formation of Rh-PCBs. As shown in Figure 1c, the treated-PF(a) displayed a higher absorbance at 410 nm than the treated-PF(b), indicating that LU treatment induced a fast diffusion of rhodium ions and therefore results in the formation of high concentration of Rh-PCBs in treated-PF(a) (concentration of treated-PF(a): 3.8×10^{-6} mol·g^{-1}; concentration of treated-PF(b): 3.2×10^{-6} mol·g^{-1},

which were calculated according to UV-VIS standard curve (Figure S13)). These results confirmed the acceleration of the ligand exchange rate of Rh-PCBs by cavitation.

With the understanding that CMF can cause the dissociation of aggregates of micro-phase separated morphology and accelerate the ligand exchange rate of Rh-PCBs, we speculated that when a deformed Rh-IMP-D(*x*) under application of an external force is treated by LU, the topology of the molecular switches in the deformed Rh-IMP-D(*x*) can rearrange rapidly, resulting in the formation of a new topology of molecular switches in the deformed Rh-IMP-D(*x*). A "deformation experiment" was designed and performed to prove this speculation. As shown in Figure 1d, in the experiment, a straight strip (20mm×1.5mm×1.5mm) of Rh-IMP-D(*7*) was folded to an angle of 0° and kept in this shape under an external force. The deformed polymer strip was afterwards treated by LU (amplitude: 80%, 3 min, in water at constant 18 ± 1 °C), this was to ensure that the topological rearrangement of the molecular switches in Rh-IMP-D(*7*) can take place during deformation while treated with LU. After LU treatment, the external force was removed and a fixed angle of 100° was obtained. In addition, two sets of experiments were designed as control. In the control (a), the strip of Rh-IMP-D(*7*) was firstly treated by LU (same LU condition as experimental), and afterwards folded to an angle of 0° and kept in this shape for 3 min. In this manner, firstly, the LU treatment made the molecular switches of Rh-IMP-D(*7*) in a non-equilibrium state (dissociation of micro-phase morphology and acceleration of ligand exchange rate of Rh-PCBs). After LU treatment, the strip of Rh-IMP-D(*7*) was deformed, enabling the topology of molecular switches to rearrange at the non-equilibrium state (no further LU treatment) under deformation. Removal of external force resulted in a fixing angle of around 140°. In the control (b), the strip was directly folded to an angle of 0° and kept this shape in water (constant 18 ± 1 °C) for 3 min (to exclude the influence of LU on the topological rearrangement of molecular

switches). A fixing angle of around 160° was obtained after removal of the external force. The obtained fixing angle after programming reflects the capability of forming a new topology of molecular switches. A fixing angle indicates a faster topological rearrangement of the molecular switches. Therefore, the lower fixing angle (100°) obtained from the experiment confirmed that the topology of molecular switches in Rh-IMP-D(*x*) is much easier to rearrange under deformation state during LU treatment. In contrast, the fixing angle (160°, low fixity) from control (b) specimen without LU treatment indicated an almost unchanged topology of molecular switches. From the perspective of the shape-memory mechanism, the rapidly topological rearrangement of molecular switches is beneficial for shape fixation. Thus, using LU to treat the deformed Rh-IMP-D(*x*) was employed to fix the temporary shape for the next shape-memory tests. However, the fixing angle of 100° in the experiment also substantially lower compared to the programming angle of 0°. This can be attributed to the non-equilibrium state of molecular switches after LU treatment (dissociation of aggregates of micro-phase separated morphology and the accelerated ligand-exchange of Rh-PCBs). Therefore, to obtain a better shape fixity, after LU treatment, the deformed Rh-IMP-D(*x*) under application of an external force must be maintained for an equilibration time period to enable the re-aggregation of micro-phase separated morphology and a decreased ligand-exchange rate of Rh-PCBs.

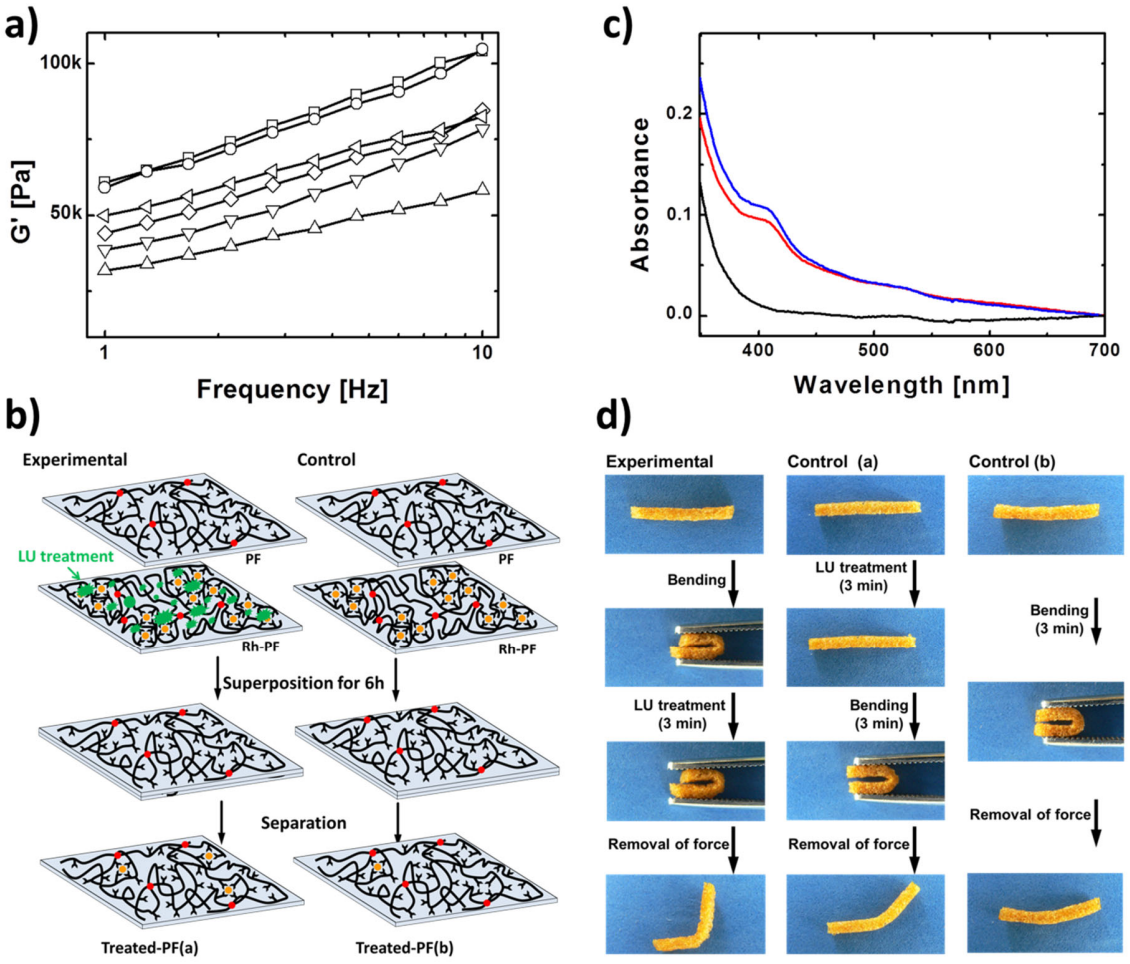

Figure 1. a) Frequency-dependent storage moduli of Rh-IMP-D(9). Hollow square: without LU treatment, first measurement; hollow circle: without LU treatment, second measurement; hollow up triangle: after LU treatment (LU amplitude: 80%, period of LU treatment: 15 min, in water at constant 18 ± 1 °C); hollow down triangle: 2 h after LU treatment; hollow diamond: 4 h after LU treatment; hollow left triangle: 6 h after LU treatment. Samples for rheology test: discs (20 mm in diameter and 1 mm in thickness). b) Schematic illustration of rhodium ion diffusion experiment. c) UV-VIS spectra of PF (black solid line), treated-PF(a) (blue solid line), and treated-PF(b) (red solid line). d) Photographs of deformation experiment.

According to the reversible dissociation of the micro-phase separated morphology and acceleration of ligand change rate of Rh-PCBs before and after LU treatment, we expected that the Rh-IMP-D(x) is capable of SME. A bending test was performed to explore the shape-memory behavior of the Rh-IMP-D(x). A straight strip of Rh-IMP-D(x) was folded to an angle 0° and then treated by LU (3 min, amplitude 80%, in water at constant 18 ± 1 °C), an external force was applied to keep the deformed shape during LU treatment. Afterwards, the LU was switched off and the deformed strip was equilibrated under the external force for a controlled fixing time period (ranging between 2 h and 12 h). Finally, a temporary shape was obtained after removal of the external force and the shape fixity ratio (R_f) was calculated. In the shape recovery experiment, the temporary shaped sample was exposed to LU (amplitude 80%, in water at constant 18 ± 1 °C) for 30 min, from which the recovered permanent shape was obtained and the shape recovery ratio (R_r) was calculated. The influence of the fixing time period on the R_f was investigated (Figure 2a). It can be observed that the increase of fixation time resulted in the increase in R_f value, and the R_f values of all Rh-IMP-D(*x*) reached equilibrium after fixing time of 4 h. Additionally, the values of R_f exhibited significant increase with the increase of DPPST composition in Rh-IMP-D(x), which can be attributed to the high DPPST composition enabling high coordination crosslink density in Rh-IMP-D(x). Furthermore, as listed in Table 1, all Rh-IMP-D(*x*) (fixing time of 4 h) exhibited similar R_f and R_r values in the three programming/recovery cycles, indicating a repeatable shape-memory performance. In addition, the poor shape fixity of Rh-IMP-D(*5*) and the poor shape recovery of Rh-IMP-D(*13*) implied that the DPPST composition ranging between 7 mol% and 11 mol% was an optimum composition to achieve the CMF-induced SME. The influence of the LU amplitude on the R_r values was also studied (Figure 2b). Higher LU amplitudes resulted in higher R_r values as an increase of LU amplitude enhances the cavitation intensity. Typical photographs to

demonstrate the LU-triggered SME are presented in Figure 2c. Moreover, the infrared photography confirmed that the SME of Rh-IMP-D(x) was not thermally induced (Figure S14).

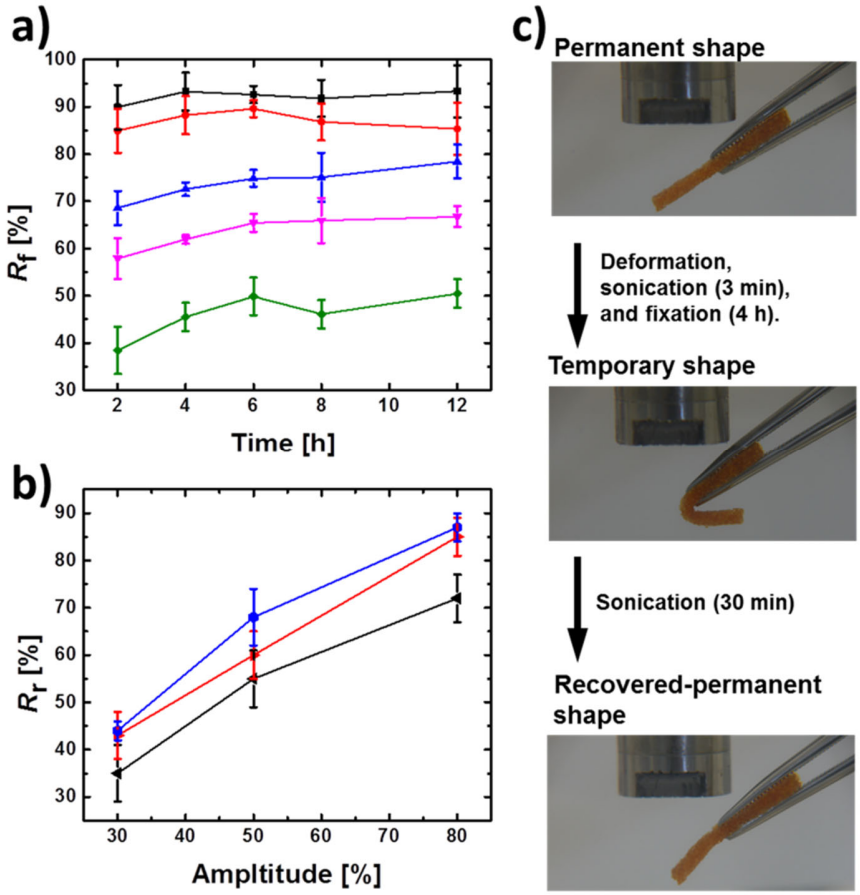

Figure 2. a) Influence of the fixing time period on the shape fixity ratio (R_f) of Rh-IMP-D(x). Black square: Rh-IMP-D(*13*), red circle: Rh-IMP-D(*11*), blue up triangle: Rh-IMP-D(*9*), magenta down triangle: Rh-IMP-D(*7*), and green diamond: Rh-IMP-D(*5*). b) Influence of the ultrasound amplitude on the recovery ratio (R_r) of Rh-IMP-D(*x*). Black left triangle: Rh-IMP-D(*11*), red right triangle: Rh-IMP-D(*9*), and blue hexagon: Rh-IMP-D(*7*). d) Photographs of Rh-IMP-D(*9*) to demonstrate the CMF-induced SME.

Table 1. R_f and R_r values of Rh-IMP-D(*x*) within three CMF-induced programming/recovery cycles.

Sample-ID	R_f, 1st [%]	R_r, 1st [%]	R_f, 2nd [%]	R_r, 2nd [%]	R_f, 3rd [%]	R_r, 3rd [%]
Rh-IMP-D(*13*)	93 ± 4	55 ± 7	87 ± 5	51 ± 4	85 ± 4	55 ± 9
Rh-IMP-D(*11*)	88 ± 4	75 ± 9	88 ± 1	78 ± 8	84 ± 6	78 ± 7
Rh-IMP-D(*9*)	72 ± 2	85 ± 5	74 ± 3	90 ± 8	77 ± 2	87 ± 2
Rh-IMP-D(*7*)	62 ± 1	87 ± 5	58 ± 4	90 ± 9	56 ± 1	90 ± 5
Rh-IMP-D(*5*)	45 ± 3	95 ± 1	40 ± 4	94 ± 2	43 ± 3	97 ± 4

3. Conclusions

In summary, we designed and prepared the Rh-IMP-D(*x*), which can exhibit CMF-induced SME upon LU treatment. In this Rh-IMP-D(*x*), the Rh-PCBs as well as their micro-phase separated morphology are provided as molecular switches (temporary crosslinks). The CMF can reversibly dissociate the micro-phase morphology and accelerate the ligand change rate of Rh-PCBs. Therefore, once the deformed Rh-IMP-D(*x*) is treated by LU, the topology of molecular switches in Rh-IMP-D(*x*) is capable to undergo a rapid rearrangement, which enables the deformed polymer backbones in Rh-IMP-D(*x*) to relax stress. In this way, the temporary shape of Rh-IMP-D(*x*) can be fixed. Subsequent exposure of the temporary shape to LU results in the re-dissociation of the micro-phase separated morphology, re-increase of ligand exchange rate of Rh-PCBs, and the covalent netpoints enables the Rh-IMP-D(*x*) to return its permanent shape. Potential applications of Rh-IMP-D(*x*) could be mechano-sensors or ultrasound controlled switches. However, we

believe that the concept of the CMF-induced SMP affects the research field of SMPs and inspires creativity of designers and engineers.

Supporting Information:

Supporting Information is available from the Wiley Online Library or from the author.

Acknowledgements:

This work has been financially supported by the Helmholtz Association through programme-oriented funding and the Tianjin University-Helmholtz-Zentrum Geesthacht, Joint Laboratory for Biomaterials and Regenerative Medicine, which is financed by the German Federal Ministry of Education and Research (BMBF, Grant No. 0315496) and the Chinese Ministry of Science and Technology (MOST, 2008DFA51170).

Keywords: ultrasound, cavitation based mechanical force, shape-memory polymer, rhodium-phosphine coordination bonds, interconnected macro-porous structure

[1] S. Mitragotri, *Nat. Rev. Drug. Discov*. **2005**, 4, 255.
[2] D. G. Shchukin, E. Skorb, V. Belova, H. Mohwald, *Adv. Mater*. **2011**, 23, 1922.
[3] J. M. J. Paulusse , R. P. Sijbesma, *J. Polym. Sci. Pol. Chem*. **2006**, 44, 5445.
[4] R. Pecha, B. Gompf, *Phys. Rev. Lett*. **2000**, 84, 1328.
[5] M. Dular, B. Bachert, B. Stoffel, B. Sirok, *Wear* **2004**, 257, 1176.
[6] S. Mitragotri, J. Kost, *Biotechnol. Progr*. **2000**, 16, 488.
[7] S. Mitragotri, D. Blankschtein, R. Langer, *Science* **1995**, 269, 850.
[8] A. H. Mesiwala, L. Farrell, H. J. Wenzel, D. L. Silbergeld, L. A. Crum, H. R. Winn, P. D. Mourad, *Ultrasound. Med. Biol*. **2002**, 28, 389.
[9] Z. L. Wu, B. Ondruschka, A. Stark, *J. Phys. Chem. A*. **2005**, 109, 3762.
[10] M. K. Beyer, H. Clausen-Schaumann, *Chem. Rev*. **2005**, 105, 2921.
[11] A. Piermattei, S. Karthikeyan, R. P. Sijbesma, *Nat. Chem*. **2009**, 1, 133.
[12] J. M. J. Paulusse, D. J. M. van Beek, R. P. Sijbesma, *J. Am. Chem. Soc*. **2007**, 129, 2392.
[13] T. Xie, *Polymer* **2011**, 52, 4985.
[14] Q. Zhao, H. J. Qi, T. Xie, *Prog. Polym. Sci*. **2015**, 49-50, 79.
[15] M. Behl, M. Y. Razzaq, A. Lendlein, *Adv. Mater*. **2010**, 22, 3388.
[16] J. R. Kumpfer, S. J. Rowan, *J. Am. Chem. Soc*. **2011**, 133, 12866.
[17] A. Lendlein, S. Kelch, *Angew. Chem. Int. Edit*. **2002**, 41, 2034.
[18] Q. Zhao, W. K. Zou, Y. W. Luo, T. Xie, *Sci. Adv*. **2016**, 2, e1501297.

[19] N. Zheng, Z. Fang, W. Zou, Q. Zhao, T. Xie, *Angew. Chem. Int. Edit*. **2016,** 55, 11421.
[20] J. A. Long, T. B. Marder, P. E. Behnken, M. F. Hawthorne, *J. Am. Chem. Soc*. **1984**, 106, 2979.